ARL-TN-1022 ● JUNE 2020

DEVCOM ARMY RESEARCH LABORATORY

Some Numerical Considerations for Shock Simulations of Ceramics

by Richard Becker

NOTICES

Disclaimers

The findings in this report are not to be construed as an official Department of the Army position unless so designated by other authorized documents.

Citation of manufacturer's or trade names does not constitute an official endorsement or approval of the use thereof.

Destroy this report when it is no longer needed. Do not return it to the originator.

ARL-TN-1022 ● JUNE 2020

Some Numerical Considerations for Shock Simulations of Ceramics

Richard Becker
Weapons and Materials Research Directorate, CCDC Army Research Laboratory

REPORT DOCUMENTATION PAGE

Form Approved
OMB No. 0704-0188

1. REPORT DATE *(DD-MM-YYYY)*	2. REPORT TYPE	3. DATES COVERED (From - To)
June 2020	Technical Note	May 2020–June 2020

4. TITLE AND SUBTITLE
Some Numerical Considerations for Shock Simulations of Ceramics

5a. CONTRACT NUMBER

5b. GRANT NUMBER

5c. PROGRAM ELEMENT NUMBER

6. AUTHOR(S)
Richard Becker

5d. PROJECT NUMBER

5e. TASK NUMBER

5f. WORK UNIT NUMBER

7. PERFORMING ORGANIZATION NAME(S) AND ADDRESS(ES)
CCDC Army Research Laboratory
ATTN: FCDD-RLW-B
Aberdeen Proving Ground, MD 21005

8. PERFORMING ORGANIZATION REPORT NUMBER
ARL-TN-1022

9. SPONSORING/MONITORING AGENCY NAME(S) AND ADDRESS(ES)

10. SPONSOR/MONITOR'S ACRONYM(S)

11. SPONSOR/MONITOR'S REPORT NUMBER(S)

12. DISTRIBUTION/AVAILABILITY STATEMENT
Approved for public release; distribution is unlimited.

13. SUPPLEMENTARY NOTES
ORCID ID: 0000-0003-0104-856X

14. ABSTRACT

A comparison of the analytic solution for interface velocity at a planer impact interface with a momentum-conserving numerical contact algorithm suggests a guideline for setting the relative element sizes on either side of the interface. Scaling the element size by the sound speed is shown to produce an initial interface velocity consistent with the Rankine–Hugoniot solution. This introduces a smaller initial perturbation into the numerical simulation, and less noise is generated and propagated from the contact surface. The damping of the subsequent residual numerical noise by the traditional artificial bulk viscosity construct is also briefly examined. Damping by the linear artificial bulk viscosity compellingly reduces noise in elastic materials for coefficients greater than 0.1. A coefficient of 0.2 substantially reduces the noise, but viscous damping this strong will noticeably broaden the shock front.

15. SUBJECT TERMS
shock, impedance, contact, mesh, bulk viscosity, numerical damping

16. SECURITY CLASSIFICATION OF:			17. LIMITATION OF ABSTRACT	18. NUMBER OF PAGES	19a. NAME OF RESPONSIBLE PERSON
a. REPORT	b. ABSTRACT	c. THIS PAGE			Richard Becker
Unclassified	Unclassified	Unclassified	UU	18	19b. TELEPHONE NUMBER (Include area code) 410-278-7980

Contents

List of Figures

List of Tables

1. Introduction

Numerical methods have long been used to analyze and understand deformation and failure in materials and structures. Analysts utilize best practices and informal guidance accumulated over many years to get relevant solutions with minimal, or at least known, numerical artifacts. Theory and experiments serve as standards for verification, validation, and sanity checks on solution quality. Parameter studies varying the numerical discretization and algorithms are used to assess the influence of algorithmic features.

For the Department of Defense, most of the historical guidance for setting numerical parameters for impact simulations comes from experience on metals. Metals generally have plastic flow strengths small in comparison to the moduli and substantial plastic dissipation that quiets stress waves and numerical noise. When running impact simulations of metals on ceramics, unexpected numerically induced noise was noticed in the ceramic, which prompted this brief excursion examining how certain simulation settings might be different for analyses involving materials with substantially different sound speeds.

Several aspects of the numerical solution are discussed in this technical note. These eventually relate to guidance on mesh density across material interfaces and adequate linear artificial bulk viscosity values to quell contact noise in elastic materials.

2. Physics and Numerical Treatment

Two aspects of shock impact and the corresponding numerical algorithms will be presented briefly. These are momentum conservation at interfaces and treatment of the shock discontinuity.

2.1 Momentum Conservation at Interfaces

2.1.1 Physics Solution

The impact pressure and interface velocity resulting from the normal impact of two planar surfaces is governed by the Rankine–Hugoniot momentum conservation relation. In the simplest form viewed from the laboratory reference frame, the longitudinal stress in the impactor with reference density ρ_I and moving at velocity U_I comes to equilibrium with the longitudinal stress in the initially stationary target with reference density, ρ_T (Marsh 1980):

$$\rho_I C_I (U_I - U_s) = \rho_T C_T U_S. \tag{1}$$

The U_s is the velocity of the interface, which is also the particle velocity in the target. C_I and C_T are the longitudinal sound speeds in the impactor and target, respectively.

Equation 1 can be rearranged to give the interface velocity as a function of the impact velocity and material properties:

$$U_S = U_I \frac{\rho_I\left(\frac{C_I}{C_T}\right)}{\rho_I\left(\frac{C_I}{C_T}\right)+\rho_T}. \quad (2)$$

Here, for simplicity and illustrative purposes, the dependence of sound speed on pressure is ignored.

2.1.2 Numerical Approximation

In explicit finite element codes, the interface velocity on impact is typically handled in one of two ways. In one method the contact is penalty based, where a contact stiffness and the position of the two interfaces create nodal forces that the code uses in its standard momentum calculations. Depending on the contact stiffness relative to the stiffness of the two materials, the velocities of the two interfaces can take several time steps to equilibrate. The second method, which is used in EPIC (Johnson 2011) and ALE3D (Noble et al. 2017), solves an equation for momentum conservation to determine the interface velocity on first contact.

Denoting the mass per unit interface area of the nodes on the impactor side of the interface as $\bar{m}_I$ and the corresponding velocity as u_I, and similarly denoting the mass per unit area of the nodes initially stationary target side as $\bar{m}_T$, the momenta before and after contact are equal as

$$\bar{m}_I u_I = u_s(\bar{m}_I + \bar{m}_T). \quad (3)$$

The $u_s$is the velocity of the interface after contact, which is

$$u_S = u_I \frac{\bar{m}_I}{\bar{m}+\bar{m}_T}. \quad (4)$$

Since the interface pressure is positive, there is no separation and the node on both sides of the interface continue to share a common, but evolving velocity.

2.1.3 Approach to Improve Numerical Accuracy

The similarity between Eqs. 2 and 4 is notable. If the sound speeds for the two materials are similar, as they generally are for metals, the finite element nodal calculation follows the Rankine–Hugoniot relation, provided that the nodal area masses are proportional to the densities. In a finite element model, this implies that

having the element size perpendicular to the interface be the same for both materials will give nodal velocities consistent with shock momentum conservation. Equal size elements is the general rule of thumb for metal-on-metal impact, and the heurist guidance has served the community well.

However, for metal-on-ceramic impact, and more so for polymer-ceramic interfaces, the sound speeds can easily differ by a factor of 2 to 5. For steel ($\rho_I = 7.8\,\mathrm{g/cm^3},\ C_I = 5800\,\mathrm{m/s}$) impacting boron carbide ($\rho_I = 2.57\,\mathrm{g/cm^3},\ C_I = 14000\,\mathrm{m/s}$), the interface velocity will be approximately 0.56 of the impact velocity. However, with equal-sized elements, the interface nodes in the finite element solution would have a velocity of 0.76 times the impact velocity. The disparity is greater if the steel yields plastically on impact, and the lower bulk sound speed is the applicable value. The artificially high initial nodal interface velocity is reduced over subsequent time steps, but it places an unphysical velocity perturbation into the system that can propagate far from the interface in a ceramic, which has little capacity to dissipate stress waves.

It is proposed that the finite element mesh size in the direction normal to the interface be scaled relative to the target element size by the ratio of the sound speeds to obtain initial impact interface velocities more in line with the Rankine–Hugoniot relations. For the case of steel impacting boron carbide, the element size for the steel in the direction normal to the interface should be reduced to 42% of the corresponding element dimension in the boron carbide.

An additional feature of scaling the element size by the sound speed is that the shock will traverse one element on each side of the interface in the same time. The effects of the second row of nodes will be felt at the same time, and the proportional contributions of pressure and bulk viscosity will be approximately the same on both sides of the interface. This creates a form of timing symmetry for numerical artifacts that may further reduce noise and oscillations at the interface.

2.2 Treatment of the Shock Discontinuity

Shocks present a challenge for finite element and finite difference methods because the shock width is generally much, much smaller than the numerical grid, and the state is discontinuous across the shock. It would be ideal if a shock that has traveled partway through an element would exert forces on the downstream nodes but not the upstream nodes, but the standard finite element method does not admit that possibility. Numerically, as an element is compressed by a passing shock, the stress rises gradually as the element volume changes. By the time the correct stress state is reached in the element, the nodes have significant momentum and the Hugoniot state is subsequently overshot. This sets up stress and velocity oscillation behind

the shock. To mitigate these numerical discretization effects, an algorithm is used that spreads the shock over several elements.

A bulk artificial viscosity treatment (VonNeumann and Richtmyer 1950), often called the "bulk-Q", is traditionally used both to smear the shock front and to account for the shock entropy not captured in integrating the deformation over a finite volumes of material. The treatment is generally only applied in compression and comprises terms that are linear and quadratic (e.g., Noble et al. 2017) in the volume strain rate, $\dot{V}/V$:

$$Q = \begin{cases} q_L \, \rho \, C_L \, l \left| \frac{\dot{V}}{V} \right| + q_Q \, \rho \, l^2 \left(\frac{\dot{V}}{V} \right)^2 & \text{if } \dot{V} < 0 \\ 0 & \text{otherwise} \end{cases} . \tag{5}$$

The q_L and q_Q are the linear and quadratic coefficients, C_L is the longitudinal sound speed, and l is a characteristic element length. The Q is added along with the pressure when computing the element nodal forces from the stress. The quadratic term is most active in strong shocks, and the linear term serves both to stiffen the material in the shock and to damp ringing coming from the shock front.

The bulk-Q should not be set high enough to exert the full shock stress. A value of $q_L = 1.0$ would make Q roughly equal to the shock pressure expected at an impact interface. However, the bulk-Q also pushes on the nodes on the unshocked side of the element, causing them to accelerate prematurely. This can spread the shock over many elements and make it propagate too quickly. Generally, a smaller value of q_L is used to account for some of the shock stress without unduly spreading the shock front. A default value of $q_L = 0.06$ is used by Abaqus/Explicit and $q_L = 0.2$ is used by EPIC. These lower values control oscillations from the shock front but do not eliminate them.

In a further effort to control the oscillations behind a shock, Christensen (1990) proposed a "Monotonic-Q" treatment motivated by a Godunov method. This algorithm replaces the volume strain rate with a velocity gradient and creates a separate function on either side of the shock. Algorithmic monotonicity constraints are enforced when evaluating the gradient to ensure there are no local extrema, and the linear contribution to the gradient is removed to limit numerical diffusion. This provides an operator that is fairly localized to the shock region. There are also tensor-Q treatments that account for the orientation of the shock front (e.g., Kolev and Rieben 2009), but these are more complicated and not generally available.

2.3 Demonstration Problem Description

A simple one-dimensional shock problem was constructed to illustrate the mesh and bulk-Q effects on stress oscillations behind a shock. Three material layers are simulated. A steel plate impacts a stationary ceramic target backed by a polymer. The goal is to investigate the artificial ringing in the ceramic, so in all of the simulations, the 8-mm-thick ceramic target is discretized with 40 uniformly spaced constant stress hexahedral elements. This discretization is similar to what would be used in a full-scale analysis of a large system. The steel impactor and polymer backing were also discretized with hexahedral elements. These element sizes were either the same 0.2-mm size as the ceramic or they were scaled by the ratio of the sound speeds. The configuration with the scaled elements is shown in Fig. 1. The scaled elements in the steel were 0.42 the thickness of the ceramic elements, and the scaled polymer elements were 0.34 of the thickness of the ceramic elements. The simulations are focused on early times. They do not include the effect of waves reflected from either the steel or polymer free surfaces, so the thicknesses of these layers do not impact the results.

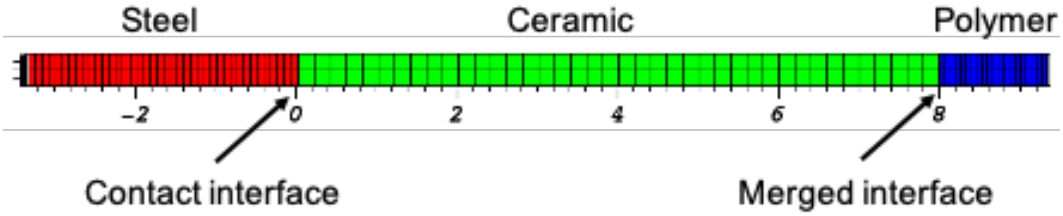

Fig. 1 Mesh and material layout for shock simulations

The cross section contains two elements in each of the two lateral directions. To simulate uniaxial strain from a shock, the lateral faces were constrained from motion normal to the surfaces, and the nodes were unconstrained along the shock direction. The steel and the ceramic had separate nodes at the contact interface, but the ceramic and the polymer shared nodes at the interface near the right end of the model. The finite element model was run in ALE3D (Noble et al. 2017) with a 900 m/s impact velocity.

The ceramic is not permitted to fracture in these simulations. The yield strengths of the steel and ceramic are artificially high to keep them elastic; the polymer has a low yield strength; and the polymer also includes significant nonlinearity in the equation of state (EOS). The material properties used in the simulations are listed in Table 1. Here, ρ is the density, K the bulk modulus, Γ the Grüneisen coefficient, G the shear modulus, and σ_y the yield strength. The S_1, S_2, and S_3 are the linear, quadratic, and cubic coefficients describing the dependence of the shock velocity on the particle velocity for the Grüneisen EOS.

Table 1 Material parameters used in the shock simulations

Mat.	ρ (g/cm^3)	K (GPa)	S_1	S_2	S_3	Γ	G (GPa)	σ_y (MPa)
Steel	7.82	163.9	1.33	0	0	1.67	77.5	2.e6
Ceramic	2.51	233.2	1.53	0	0	1.28	197	2.e6
Polymer	1.19	4.69	3.49	–8.2	9.6	0.61	4.49	0.12

The simulations examining the mesh effects at the interfaces all used a linear bulk viscosity coefficient of $q_L = 0.2$. Calculations exploring the artificial bulk viscosity effects all used the scaled mesh configuration and linear coefficients of $q_L = 0.1$ and $q_L = 0.2$. In addition, the Monotonic-Q option in ALE3D was exercised for comparison.

3. Results

The simulations were run to 800 ns, and plots of the longitudinal stress along the specimen thickness were extracted. The impact interface is initially at a coordinate of zero, and the interface between the ceramic and the polymer is at 8 mm.

3.1 Effect of Element Size

The effect of the element size in the steel impactor is shown in Fig. 2. The times are indicated above the legends. The results for the uniform mesh are shown in green, and those from the scaled mesh are red dashes. Three overall features are notable. First is that the wave running through the ceramic to the right is traveling much faster than the left-traveling wave in the steel. Second is that the stress perturbations tend to decay over time. Third is that the left-traveling shock front in the steel is steeper with the smaller element size of the scale mesh.

At 20 ns, in Fig. 2a, the higher initial interface velocity resulting from the nodal momentum conservation with the uniform mesh created a stress in excess of 20 GPa. This is higher than the stress from the Rankine–Hugoniot equations. The more accurate initial velocity from the scaled elements did not cause a significant stress overshoot. By 80 ns, Fig. 2b, the stress rebound from the initial perturbation with the uniform mesh has created a stress pulse of a few gigapascals trailing the right-traveling shock. The magnitude of the perturbation in the simulation with the scaled mesh in the steel is about half as great. At the two later times the linear artificial bulk viscosity has substantially damped the stress perturbation in both simulations. This will be described in more detail in Section 3.2.

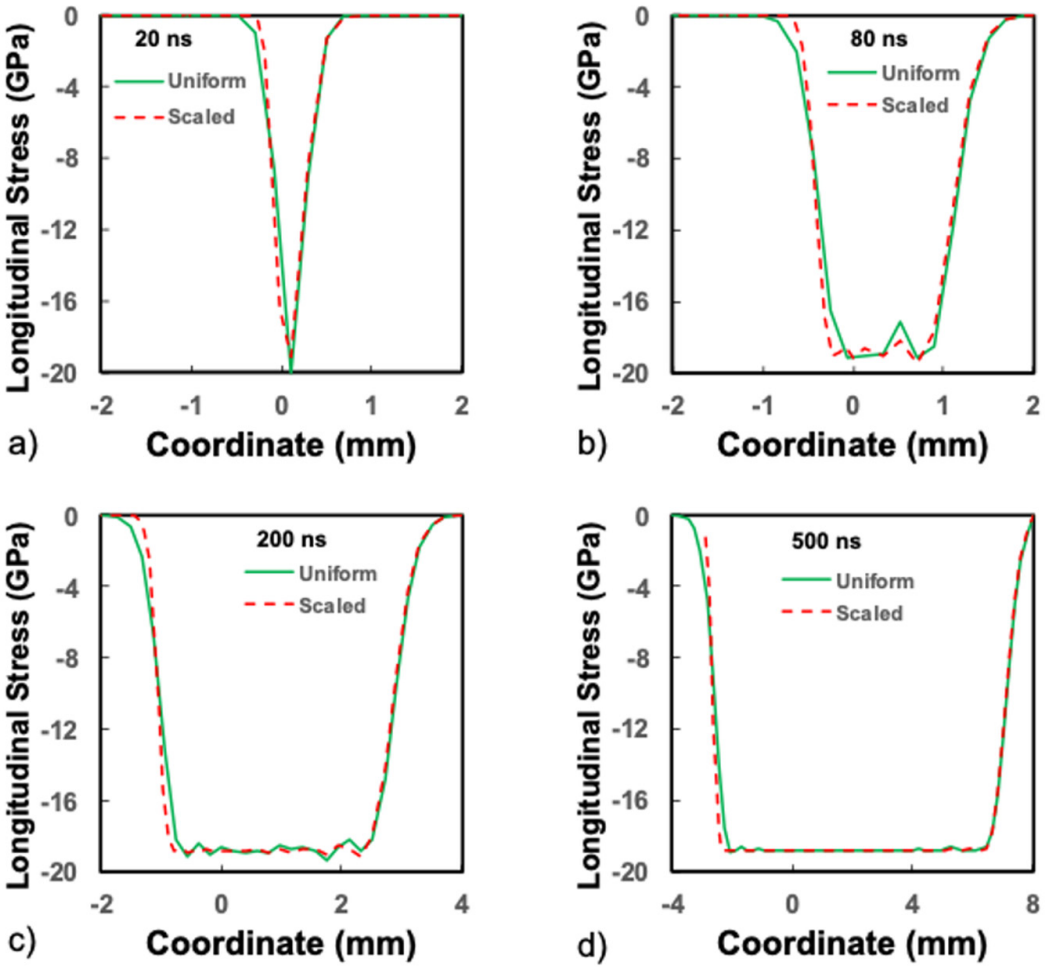

Fig. 2 Longitudinal stress distribution at a) 20 ns, b) 80 ns, c) 200 ns, and d) 500 ns. The impact interface is at zero.

The effect of the mesh size at the initially stationary ceramic-polymer interface at the right of the model is not as dramatic because the diffuse shock front ramps the velocities more gradually. In Fig. 3, the shock has reflected from the ceramic-polymer interface at the 8-mm coordinate, and the resulting partial-release wave is traveling left in the ceramic. The wave beyond 8 mm is traveling to the right in the polymer. While the stress perturbation is smaller than at the impact interface, having the mesh scaled appropriately with the sound speed does reduce the size of the perturbation.

As with the steel at earlier times, the finer mesh in the polymer allows the stress gradient to be steeper. It is also evident that the wave is propagating much more rapidly in the ceramic than the polymer.

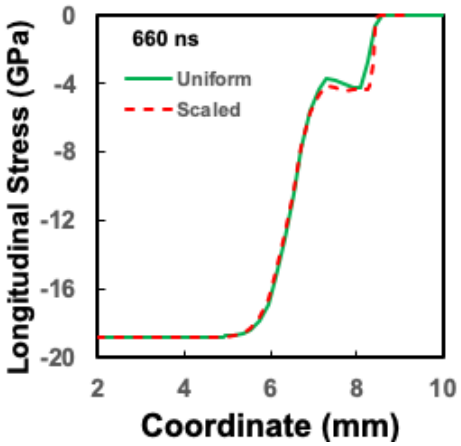

Fig. 3 Longitudinal stress distribution at 660 ns, after reflection from the ceramic-polymer interface at 8 mm

3.2 Artificial Bulk Viscosity Effects

The longitudinal stress distribution dependence on the linear bulk viscosity coefficient is presented in Fig. 4 as the blue and dashed red lines. With the lower coefficient of $q_L = 0.1$, the noise generated at the impact interface is still substantial after 200 ns. Increasing the coefficient to 0.2 quells the noise more effectively, but the slope of the curves is decreased, indicating that the higher bulk-Q value is spreading the shock over more elements. The same trends are also evident after the wave reflects from the ceramic-polymer interface, Fig. 4b. The noise is not suppressed as rapidly with the lower coefficient, and the partial release is spread over a larger number of elements with the higher bulk-Q value. It appears that linear bulk viscosity coefficients chosen between 0.1 and 0.2 will dissipate numerical noise while not unduly broadening the simulated shock front.

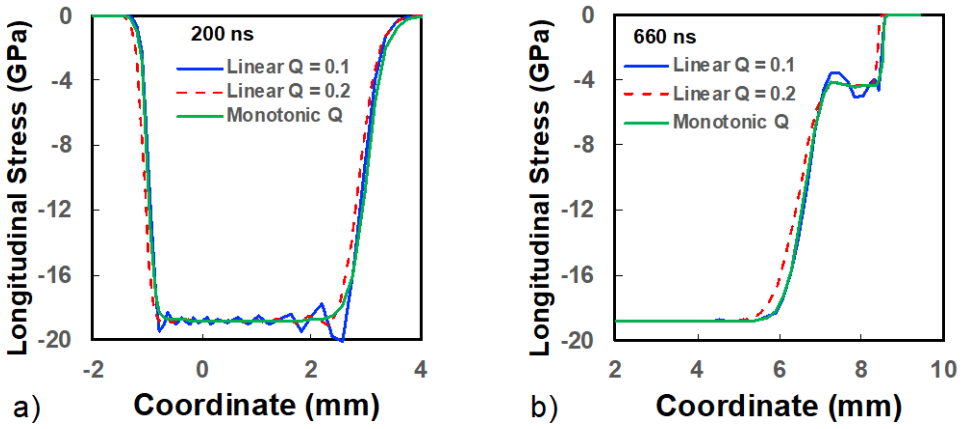

Fig. 4 Longitudinal stress profiles with different linear bulk viscosity coefficients at a) 200 ns and b) 660 ns. The noise at the earlier time originates at the impact interface and at the later time from reflection from the ceramics-polymer interface. Also included are results using the Monotonic-Q algorithm.

Also included in Fig. 4 are stress profiles using the Monotonic-Q algorithm. This method quashes the impact noise within a few nanoseconds and does this without reducing the stress gradients as much as the $q_L = 0.2$ bulk viscosity coefficient. The Monotonic-Q does, however, smooth the stress profile more as it transitions to the plateaus. This feature of the algorithm helps prevent stress overshoot.

It is notable that the Monotonic-Q does not completely flatten the reflected stress level in Fig. 4b. This is related to the significant material nonlinearity of the polymer. The shock impedance of the polymer increases with compression, which feeds back toward the interface to increase the magnitude of the interface stress slightly over time.

4. Conclusions and Recommendations

A comparison of the theoretical velocity at an impact interface with the numerical algorithm suggests that solutions will have less transient noise if the element size normal to the interface is scaled by the sound speed of the material. The reduced noise has been verified by 1-D impact simulations. It is recommended that the element sizes on either side of an impact interface be scaled by the sound speed to reduce the numerical noise on impact.

An examination of the effects of the linear bulk viscosity coefficient on noise generated at an interface suggests that a value of 0.1 will not completely reduce the noise in an elastic target. A value of 0.2 is much more effective at damping, but it also creates a wider numerical spread of the shock front. It is recommended that the linear bulk viscosity coefficient be set between 0.1 and 0.2, depending on noise level and concern about shock front broadening.

5. References

Christensen RB. Godunov methods on a staggered mesh -- an improved artificial viscosity. Proceedings of the Nuclear Explosives Code Development Conference; 1990 Nov; Monterey, CA; pp. 6–9. Lawrence Livermore Laboratories Report No.: UCRL-JC-105269.

Johnson GR, Numerical algorithms and material models for high-velocity impact computations. Int J Impact Engr. 2011;38:456–472.

Kolev TV, Rieben RN. A tenor artificial viscosity using a finite element approach. J Comp Phys. 2009;228:8336–8366.

Marsh SP. LASL shock Hugoniot data. Berkeley (CA): University of California Press; 1980.

Noble CR, et al. ALE3D: an arbitrary Lagrangian-Eulerian multi-physics code. Livermore (CA): Lawrence Livermore National Laboratories; 2017. Report No.: LLNL-TR-732040.

VonNeuman J, Richtmyer RD. A method for the numerical calculation of hydrodynamic shocks. J Appl Phys. 1950;21:232–237.

List of Symbols, Abbreviations, and Acronyms

EOS	equation of state
ρ_I	impactor density
ρ_T	target density
U_I	impactor velocity
U_T	target velocity
U_s	surface velocity
C_I	impactor sound speed
C_T	target sound speed
$\bar{m}_I$	impactor mass per interface area
$\bar{m}_T$	target mass per interface area
u_I	node velocity on impactor surface
u_T	node velocity on target surface
u_s	surface node velocity
C_I	impactor sound speed
C_T	target sound speed
V	element volume
$\dot{V}$	element volume rate
Q	artificial viscosity
q_L	linear coefficient for bulk-Q
q_Q	quadratic coefficient for bulk-Q
C_L	longitudinal sound speed
l	element characteristic length
K	bulk modulus
S_1, S_2, S_3	linear, quadratic, and cubic coefficients for Grüneisen equation
Γ	Grüneisen coefficient
G	shear modulus
σ_y	yield strength

1 (PDF) DEFENSE TECHNICAL INFORMATION CTR DTIC OCA

1 (PDF) CCDC ARL FCDD RLD CL TECH LIB

37 (PDF) CCDC ARL
C HOPPEL
R BECKER
B SCHUSTER
A TONGE
FCDD RLW LH
C EICHHORST
C MEYER
J OGRADY
D SCHEFFLER
B SORENSEN
FCDD RLW PA
S BILYK
M COPPINGER
M GRAHAM
FCDD RLW PB
J MCDONALD
P MCKEE
S SATAPATHY
S WOZNIAK
T ZHANG
FCDD RLW PC
J CAZAMIAS
R LEAVY
J LLOYD
FCDD RLW PD
R DONEY
D KLEPONIS
C RANDOW
S SCHRAML
G VUNNI
FCDD RLW PE
D HORNBAKER
J HOUSKAMP
M LOVE
FCDD RLW PG
D FOX
S KUKUCK
J STEWART
FCDD RLW MA
T BOGETTI
J STANISZEWSKI
M YEAGER
FCDD RLW MB
B LOVE
G GAZONAS
D OBRIEN

1 (PDF) SWRI T HOLMQUIST

1 (PDF) LLNL A ANDERSON